

Fluid-Structure Interaction Benchmarking using Solids4Foam

Manish Tajpuriya¹ and Chandan Bose²

¹ Aerospace Engineering, Institute of Engineering, Tribhuvan University

² Assistant Professor, Aerospace Engineering, College of Engineering and Physical Sciences, The University of Birmingham

June 13, 2026

Synopsis

This study presents a fluid-structure interaction (FSI) analysis of a flexible beam subjected to cross-flow using the solids4foam toolbox. An elastic plate attached to the bottom of a rectangular channel is investigated, with incompressible viscous fluid entering under a parabolic velocity profile ($Re = 40$).

The fluid domain follows the incompressible Navier-Stokes equations, while the solid beam employs a neo-Hookean hyperelastic model for finite strains. A strongly-coupled partitioned approach with Aitken relaxation ensures convergence at the fluid-solid interface.

Two configurations are examined: a baseline case ($U_{peak} = 0.2$ m/s, $E = 1.4$ MPa) proposed by Richter [1] and a modified case ($U_{peak} = 0.3$ m/s, $E = 10$ kPa) designed to induce larger deformations analysed by Gillebaart et al. and Tuković et al [2]. Results show steady-state displacements of 0.1 mm and 13.4 mm respectively, with drag coefficients of 1.224 and 1.235. Grid convergence and validation against benchmark solutions confirm numerical accuracy.

This work demonstrates solids4foam's capability for external flow FSI problems and provides insights into coupled flexible structure responses under varying flow and material conditions.

Keywords: Fluid-Structure Interaction, solids4foam, OpenFOAM, beam in cross-flow, hyperelasticity, partitioned solver

Contents

List of Figures	3
List of Tables	4
List of Abbreviations	5
1 Introduction	6
2 Computational Methodology	6
2.1 Problem Definition	6
2.2 Governing Equations	6
2.2.1 fluid	6
2.2.2 solid	6
2.2.3 Fluid-Solid Interface	7
2.3 Geometry and Mesh	7
2.4 Solver Setup	9
2.4.1 Fluid Setup	9
2.4.2 Solid Setup	11
2.4.3 Coupling Setup	11
2.5 OpenFOAM Implementation	11
2.5.1 Case Directory Structure	11
2.5.2 Description of Key Files and Directories	13
3 Results and Discussion	15
3.1 Convergence Test	15
3.2 Validation	17
3.2.1 Validation Against Schott et al. (2019) — Pulsating Flow Over a Bending Flexible Flap	17
3.3 Results	20
3.3.1 Comparison with Original Case ($U = 0.2$ m/s, $E = 1.4$ MPa)	23
3.4 Discussion	25
4 Conclusions	25
5 Acknowledgement	25

List of Figures

1	Computational Domain and solid Geometry	8
2	Orthogonal View of Domain	8
3	Fluid Domain Mesh	9
4	Solid Domain Mesh	9
5	OpenFOAM / solids4foam case directory structure	12
6	Grid Convergence Study	16
7	Comparison of x_1 -displacement at point $\mathbf{X} = (0.5, 0.35, 0.0)$: present solids4foam result versus Schott et al. [3] (A2-mid).	18
8	Comparison of x_1 -displacement at point $\mathbf{X} = (0.57, 0.35, -0.3)$: present solids4foam result versus Schott et al. [3] (A2-mid).	18
9	Comparison of fluid velocity magnitude at point $\mathbf{x} = (0.6, 0.52, 0.0)$: present solids4foam result versus Schott et al. [3] (A2-mid).	19
10	Comparison of fluid pressure at point $\mathbf{x} = (0.6, 0.52, 0.0)$: present solids4foam result versus Schott et al. [3] (A2-mid).	19
11	Normalised Displacement vs Normalised time	20
12	Coefficient of Drag (C_d) vs non-dimensionalised time	21
13	Mesh Morphing	21
14	Velocity Contour	22
15	Displacement and Velocity Contour	22
16	Streamline	23
17	Comparison of Drag Coefficient: Modified Case ($U=0.3$ m/s, $E=10$ kPa) vs Original Case ($U=0.2$ m/s, $E=1.4$ MPa)	24
18	Comparison of Normalized Streamwise Displacement: Modified Case vs Original Case	24

List of Tables

1	Boundary Conditions for fluid domain	9
2	Boundary Conditions for solid domain	10
3	Finite Volume Schemes for Fluid	10
4	Number of cells for different meshes	15
5	Values with respect to different mesh sizes	16
6	Relative Error with respect to Richardson extrapolated value	16
7	Comparison of Steady-State Values	24

List of Abbreviations

FSI	Fluid-Structure Interaction
ALE	Arbitrary Lagrangian-Eulerian
CFD	Computational Fluid Dynamics
FVM	Finite Volume Method
FEM	Finite Element Method
NS	Navier-Stokes
Re	Reynolds Number
PISO	Pressure Implicit with Splitting of Operators
SIMPLE	Semi-Implicit Method for Pressure-Linked Equations
GAMG	Generalised Algebraic Multi-Grid
PBiCG	Preconditioned Bi-Conjugate Gradient
DILU	Diagonal Incomplete LU decomposition
GCI	Grid Convergence Index
CFL	Courant-Friedrichs-Lewy number
COTS	Commercial Off-The-Shelf
DOF	Degrees of Freedom
BCs	Boundary Conditions

1 Introduction

With a large number of features, including advanced algorithms for solid–fluid and thermo–solid–fluid coupling, a range of solid material models, many discretisation and solution methods for solid mechanics, and a variety of non-trivial solid boundary conditions, solids4foam [4] is a dedicated toolbox for carrying out fluid–solid interaction and solid mechanics simulations in the popular OpenFOAM software.

A flexible, extensible approach to fluid–solid and solid mechanics in OpenFOAM is enabled via the modular structure of the solids4foam toolkit, which is based on generic class interfaces for fluid dynamics, solid mechanics, coupling strategies, and solid material models cardiff2025solids4foam.

2 Computational Methodology

2.1 Problem Definition

The Fluid Solid Interaction between flexible 3D flaps and laminar incompressible flow is examined in this work. The geometry consists of a rectangular duct with a thick elastic plate fastened to its bottom surface. The fluid’s input velocity changes parabolically as the channel width increases. In this instance, a low Reynolds number flow of 40 is employed.

2.2 Governing Equations

Three sets of equations govern the fluid, solid, and interface:

2.2.1 fluid

The N-S governing equations for incompressible Newtonian isothermal laminar flow are as follows:

$$\nabla \cdot \mathbf{v} = 0 \quad (1)$$

$$\frac{\partial \mathbf{V}}{\partial t} + \mathbf{V}(\nabla \cdot \mathbf{V}) = \nu \nabla^2 \mathbf{V} - \frac{1}{\rho} \nabla p + f_b \quad (2)$$

where,

\mathbf{V} = velocity vector

f_b = force vector

ν = Kinematic viscosity

p = pressure

ρ = density

2.2.2 solid

The neo-Hookean hyperelastic law describes the material behavior under the assumption of finite strains:

$$\rho \frac{\partial^2 \mathbf{u}}{\partial t^2} = \nabla \cdot \boldsymbol{\sigma} + \rho \mathbf{g} \quad (3)$$

where,

$$\sigma = \frac{1}{J} \left[K (J^2 - 1) \mathbf{I} + \mu J^{-3} \text{dev}[\mathbf{F} \cdot \mathbf{F}^T] \right] \quad (2)$$

$$\mathbf{F} = \mathbf{I} + (\nabla_0 \mathbf{u})^T \quad (3)$$

$$\mathbf{J} = \det[\mathbf{F}] \quad (4)$$

where,

\mathbf{u} = displacement vector

σ = stress

2.2.3 Fluid-Solid Interface

At the fluid-solid interface, kinematic and dynamic conditions are maintained. According to the kinematic requirements, the displacement and velocity must be continuous throughout the interface:

$$\mathbf{v}_{fluid}^{[i]} = \mathbf{v}_{solid}^{[i]} \quad (4)$$

$$\mathbf{u}_{fluid}^{[i]} = \mathbf{u}_{solid}^{[i]} \quad (5)$$

The dynamic conditions indicate that the forces are in equilibrium and are derived from linear momentum conservation:

$$\mathbf{n}^{[i]} \cdot \sigma_{fluid}^{[i]} = \mathbf{n}^{[i]} \cdot \sigma_{solid}^{[i]} \quad (6)$$

2.3 Geometry and Mesh

A horizontal channel of size $h = 0.4\text{m}$ x $L = 1.5\text{m}$ x $w = 0.4\text{m}$ makes up the geometry. At the bottom of the channel 0.45 meters from the intake there is a flexible flap of $t(\text{thickness}) = 0.1\text{ m}$ x $h(\text{height}) = 0.2\text{m}$ x $w(\text{width}) = 0.2\text{m}$ attached. Figure 1 shows the geometry. As we are dealing with symmetric geometry only half of the spatial domain is considered.

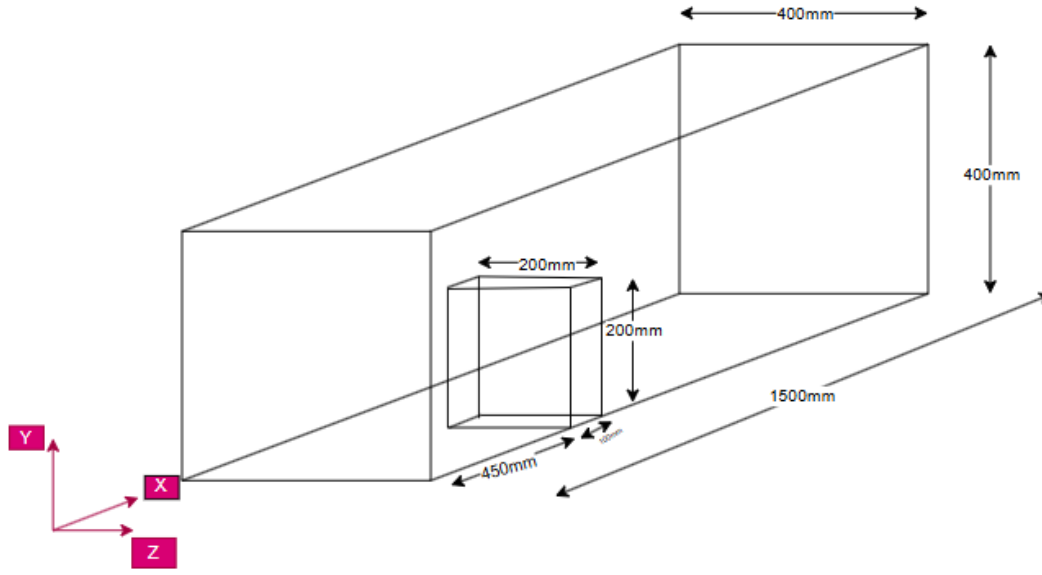


Figure 1: Computational Domain and solid Geometry

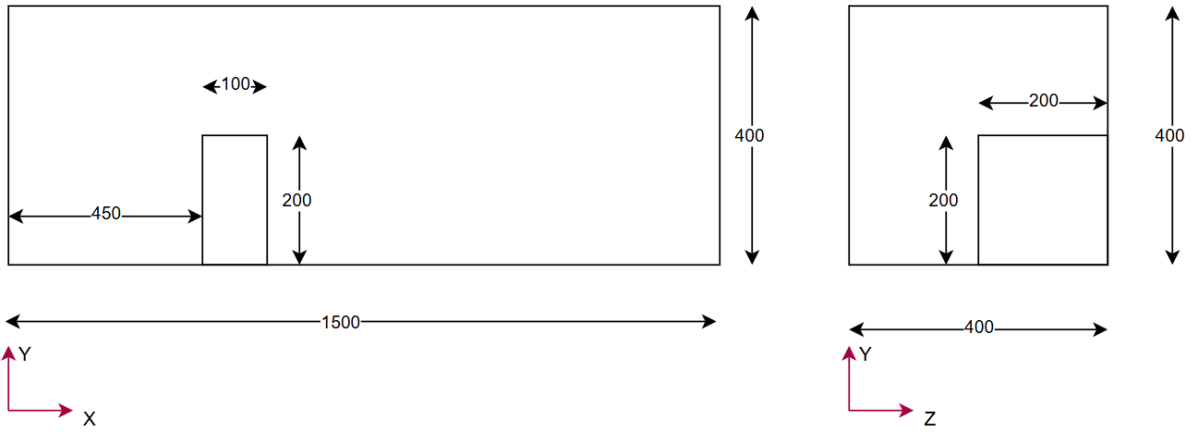


Figure 2: Orthogonal View of Domain

OpenFoam BlockMesh Utility is used for meshing. Since the fluid domain and solid in the FSI issue are solved using different equations, they should be meshed independently when employing the partitioned approach. As illustrated in Figure 3, the fluid domain is split into eleven distinct blocks, and a finer mesh is created close to the solid using simple grading. As seen in Figure 4, a solid domain is also meshed by treating it as a single block. The fluid and solid domains are meshed using only hexahedral cells.

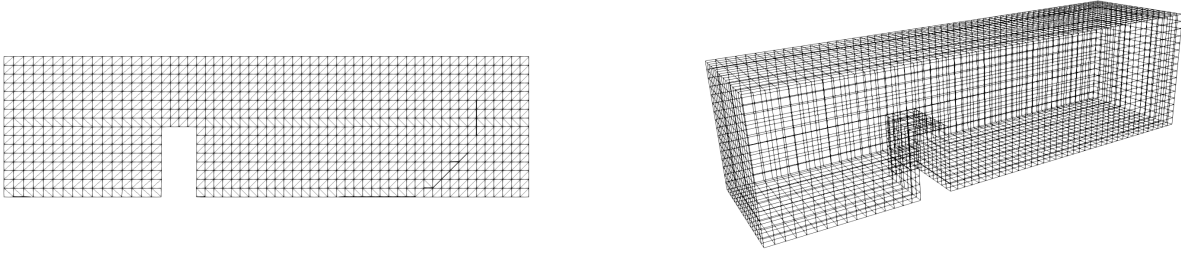


Figure 3: Fluid Domain Mesh



Figure 4: Solid Domain Mesh

2.4 Solver Setup

Fluid Setup, Solid Setup, and Coupling Setup are the three components that make up the solver setup:

2.4.1 Fluid Setup

2.4.1.1 Initial and Boundary Conditions

In relation to the plate height ($h = 0.2$ m), the maximum inflow velocity is 0.2 m/s, or $Re = 40$. The peak inlet velocity gradually increases from zero at $t = 0$ s to its maximum value at $t = 4$ s using the transition function $0.2[1 - \cos(\pi t/4)]/2$. The channel outlet is subject to a constant pressure, and the channel walls are subject to a no-slip boundary condition. The boundary conditions are given in the tables 2 and 1:

Table 1: Boundary Conditions for fluid domain

Patch	Velocity	Pressure
inlet	paraboloidInletVelocity	zeroGradient
outlet	zeroGradient	fixedValue
interface	newmovingWallVelocity	zeroGradient
bottom	noSlip	zeroGradient
top	noSlip	zeroGradient
left	noSlip	zeroGradient
symmetry	symmetry	symmetry

Table 2: Boundary Conditions for solid domain

Patch	Point Displacement
interface	solidTraction
bottom	fixedDisplacement
symmetry	solidSymmetry

2.4.1.2 Fluid properties

The fluid is considered to have a density of 1000 kg/m^3 . Equation 5 is used to determine the fluid's kinematic viscosity based on the Reynolds number value, which is 40.

$$Re = (\text{meanvelocity.length})/\text{kinematicviscosity} \quad (5)$$

Using a length scale of 1 m and a mean velocity of 0.2 m/s, the kinematic viscosity value is calculated to be $1e - 3 \text{ m}^2/\text{s}$. It is assumed that the flow is in the laminar regime.

2.4.1.3 Dynamic Mesh Treatment

Solids4Foam uses a mesh morphing technique to update the mesh on a regular basis when the solid deflects and modifies the fluid mesh. The diffusivity quadratic inverseDistance approach is used to handle the mesh motion using the VelocityLaplacian Solver.

2.4.1.4 Finite Volume Schemes

Table 3 contains a tabulation of operations and associated schemes.

Table 3: Finite Volume Schemes for Fluid

Operation	Schemes
Time Derivative	Backward
Gradient	Least Square
Divergence	default none; div(phi,U) Gauss linearUpwind cellLimited leastSquares 1; div((nuEff*dev2(T(grad(U)))) Gauss linear; div((nuEff*dev(T(grad(U)))) Gauss linear;
Laplacian	Guass Linear Corrected
Surface Normal Gradient	Corrected
Interpolation	skewCorrected Linear

2.4.1.5 Solution Method and Control

For pressure, a GAMG solver is employed, and for velocity, a PBiCG solver with a DILU preconditioner is utilized. Cell displacement and velocity are solved using the symGaussSeidal smoother in smoothSolver. There is a $1e-6$ tolerance for pressure, velocity, and cell displacement.

2.4.2 Solid Setup

2.4.2.1 Boundary Conditions

The flap functions like a cantilever beam with one end fixed firmly to the channel's bottom and the other end free to deflect. It is forbidden for the flap to deflect in the z direction. The flap deflects when the fluid applies pressure and viscous force, and it eventually becomes steady when the flow is fully formed. Because of the symmetry to reduce the computing cost, the domain features a symmetry patch.

2.4.2.2 Material properties

The density ratio of solid and fluid is considered to be 1. The material properties of the 3D flap i.e. solid are listed below:

1. Density = 1000 kg/m^3
2. Young's Modulus = 10 KPa
3. Poisson's ratio = 0.4

2.4.2.3 Control

Time step of 0.1 is used with endTime 4 seconds. Maximum courant number is 0.2

2.4.3 Coupling Setup

Maximum number of FSI loops per time step :All time step tolerance for FSI loop are kept constant as $1\text{e-}6$. The coupling switch on, from beginning ,relaxation factor is maintained to 0.4. If the deflection is big (as stated in the FSI case above) it will be better to use Implicit Coupling since the error from Explicit Coupling will be too big . The coupling scheme used is the AITKEN coupling scheme.

Number of FSI loop correctors for every time step is held at max. of 20. Tolerance value of the FSI loop for every time step is held at $1\text{e-}6$. The coupling is turned on from the start and relaxation factor is held at 0.4.Data is passed through the interfaces via DirectMap.

2.5 OpenFOAM Implementation

2.5.1 Case Directory Structure

The solids4foam FSI case follows the standard OpenFOAM directory layout, organised into three top-level folders—0, constant, and system—together with auxiliary postProcessing and script files. Both the fluid and solid sub-domains are maintained as separate subdirectories within each top-level folder, allowing the partitioned solver to handle each domain independently. The complete directory structure is shown in Figure 5.

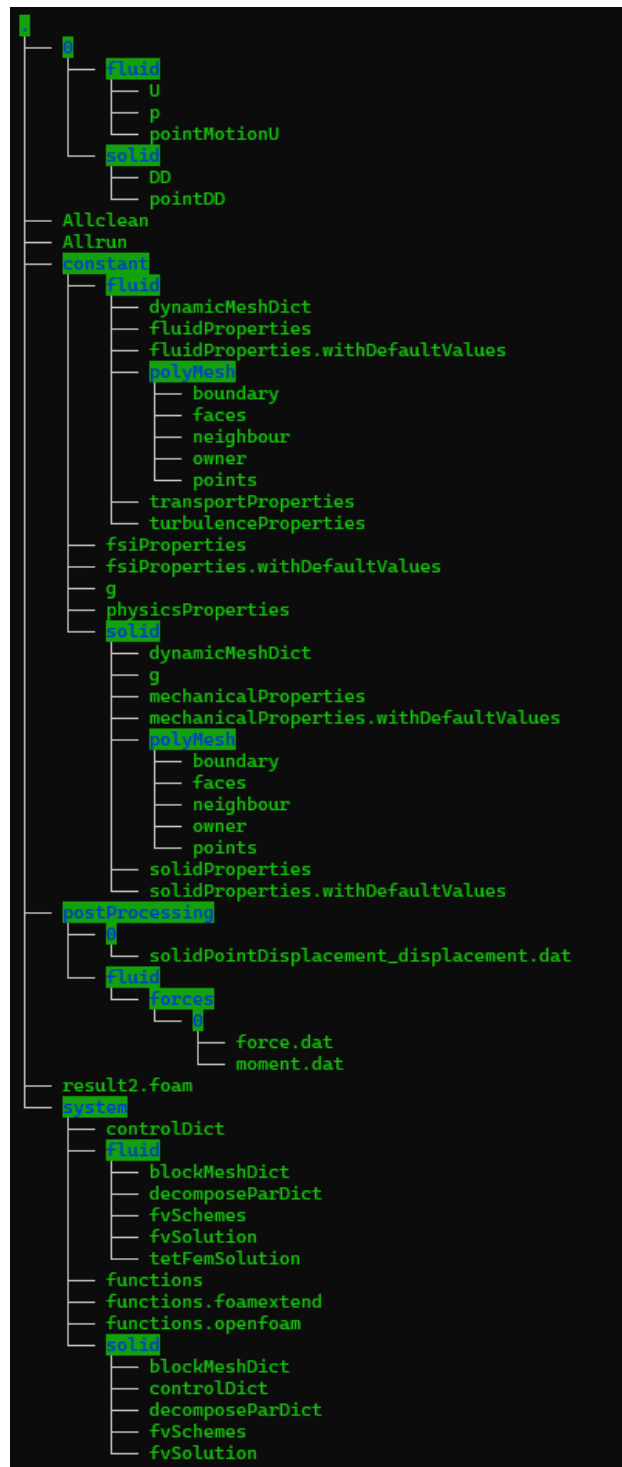


Figure 5: OpenFOAM / solids4foam case directory structure

2.5.2 Description of Key Files and Directories

2.5.2.1 The 0/ Directory — Initial and Boundary Conditions

The 0/ folder stores the state of every field at $t = 0$, split across 0/fluid/ and 0/solid/ sub-directories.

- **U** — Velocity field for the fluid subdomain. The inlet uses the custom `paraboloidInletVelocity` boundary type imposing a 3-D parabolic profile ramped from zero to U_{peak} over $t_{\text{ramp}} = 4$ s. All channel walls use `noSlip` and the FSI interface uses `movingWallVelocity` to account for mesh motion.
- **p** — Kinematic pressure field. A `fixedValue(0)` condition is applied at the outlet and `zeroGradient` elsewhere.
- **pointMotionU** — Point-velocity field used by the ALE mesh-motion solver to update fluid mesh node positions at every time step as the solid deflects.
- **DD (solid)** — Incremental displacement field for the solid subdomain, used internally by the `solids4foam` solid solver.
- **pointDD (solid)** — Point incremental displacement, used to update the solid mesh node positions consistently with the structural solution.

2.5.2.2 The constant/ Directory — Physical and Geometric Data

Fluid subdomain (constant/fluid/)

- **polyMesh/** — Complete fluid mesh topology generated by `blockMesh`: `points` (node coordinates), `faces` (face connectivity), `owner` and `neighbour` (cells sharing each internal face), and `boundary` (patch type declarations).
- **dynamicMeshDict** — Configures the `velocityLaplacian` mesh-motion solver with `quadratic inverseDistance` diffusivity, concentrating mesh distortion away from the near-wall region to preserve cell quality during large structural deflections.
- **fluidProperties / fluidProperties.withDefaultValues** — Selects the fluid solver type used by `solids4foam` (here, `icoFluid` for incompressible laminar flow).
- **transportProperties** — Specifies kinematic viscosity $\nu = 1 \times 10^{-3} \text{ m}^2/\text{s}$ and fluid density $\rho_f = 1000 \text{ kg/m}^3$, giving $Re = 40$.
- **turbulenceProperties** — Declares the turbulence model; set to `laminar` for this low-Reynolds-number case.
- **fsiProperties / fsiProperties.withDefaultValues** — Defines the coupling algorithm (Aitken relaxation), maximum FSI correctors (20), coupling tolerance (10^{-6}), and interface data-transfer method (`DirectMap`).

- **physicsProperties** — Top-level solids4foam dictionary that selects the physics type (fluidSolidInteraction) and points to the fluid and solid solver classes.
- **g** — Gravitational acceleration vector (set to zero for this horizontal-channel case).

Solid subdomain (constant/solid/)

- **polyMesh/** — Solid mesh topology (same file set as the fluid polyMesh). Meshed independently as a single hexahedral block.
- **mechanicalProperties/mechanicalProperties.withDefaultValues** — Defines the constitutive model (neo-Hookean hyperelastic), Young’s modulus E , Poisson’s ratio ν_s , and solid density ρ_s . Switching between the original ($E = 1.4$ MPa) and modified ($E = 10$ kPa) cases requires editing this file only.
- **solidProperties / solidProperties.withDefaultValues** — Selects the solid solver type used by solids4foam (here, nonLinearGeometryTotalLagrangianTotalDisplacement for finite-strain hyperelasticity).
- **dynamicMeshDict** — Solid-side mesh motion settings (minimal for the Lagrangian solid domain).
- **g** — Gravitational acceleration for the solid domain.

2.5.2.3 The system/ Directory — Numerical Setup

A top-level controlDict governs the overall simulation timeline (start time, end time, Δt , write frequency) and activates run-time post-processing functions. Fluid- and solid-specific numerical settings are placed in system/fluid/ and system/solid/ respectively.

Fluid (system/fluid/)

- **blockMeshDict** — Defines the eleven-block fluid mesh geometry, vertex coordinates, cell counts, and simple grading towards the solid interface.
- **decomposeParDict** — Sets the domain decomposition strategy for parallel runs (scotch or simple).
- **fvSchemes** — Specifies discretisation schemes for each differential operator (Table 3). Backward Euler is used for the time derivative and Gauss linearUpwind for convection.
- **fvSolution** — Sets solver types and tolerances (10^{-6}): Generalised Algebraic Multi-Grid (GAMG) for pressure and Preconditioned Bi-Conjugate Gradient (PBiCG)/Diagonal Incomplete LU decomposition (DILU) for velocity.
- **tetFemSolution** — Controls the finite-element mesh-motion solve used internally by the ALE framework.

Solid (system/solid/)

- **blockMeshDict** — Single-block solid mesh definition.
- **controlDict** — Solid-domain time-stepping parameters.
- **decomposeParDict** — Parallel decomposition for the solid.
- **fvSchemes / fvSolution** — Discretisation and solver settings for the structural equations.

Function objects (system/functions*) The files `functions`, `functions.foamextend`, and `functions.openfoam` define run-time sampled quantities. For this case it has been configured for monitoring force-coefficient on the flap surface and for writing results to `postProcessing/`.

2.5.2.4 Post-Processing and Log Files

The `postProcessing/` directory accumulates data written at run-time:

- **0/solidPointDisplacement_displacement.dat** — Time history of the tip-point displacement, used to produce the normalised displacement plots (Figures 11 and 18).
- **fluid/forces/0/force.dat** and **moment.dat** — Raw force and moment vectors on the flap, from which the drag coefficient C_D is computed (Figures 12 and 17).

The `result2.foam` file is a ParaView session file that allows direct visualisation of the coupled FSI results without additional configuration. The `Allrun` and `Allclean` scripts automate case execution and clean-up respectively, ensuring full reproducibility.

3 Results and Discussion

3.1 Convergence Test

For the Grid Convergence Test, `blockMesh` is used to create three distinct meshes. This is done to guarantee that the outcomes are unaffected by the size of the cell. The coarse, medium, and fine meshes are made using a mesh refinement factor of two. This is carried out independently for the fluid and solid domains. The Table 4 for fluid and solid separately lists the number of cells for each of the three coarse, medium, and fine mesh.

Table 4: Number of cells for different meshes

Mesh	Fluid Domain	Solid
Fine	116736	2048
Medium	14592	256
Coarse	1824	32

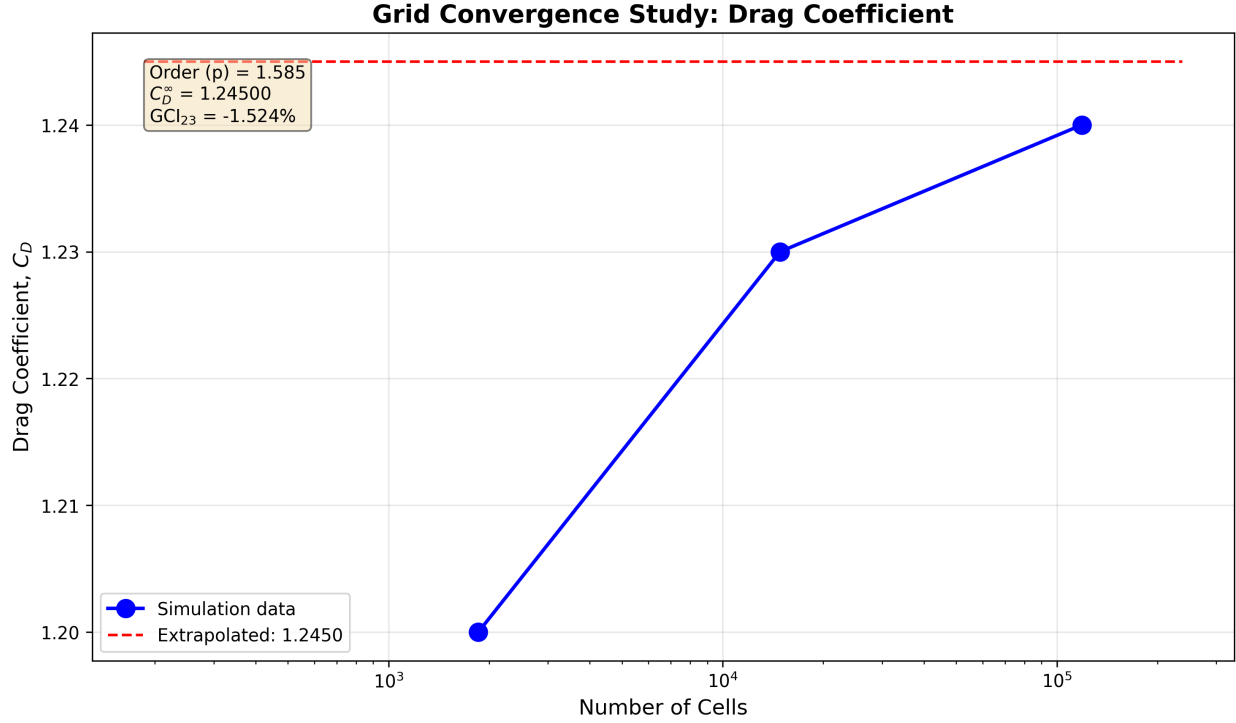


Figure 6: Grid Convergence Study

The table below lists the drag coefficient and displacement for three distinct meshes. When the cell size approaches 0, the drag coefficient values are obtained using Richardson extrapolation using the methodology described in reference [5]. In the fluid and solid realm, this should ideally imply an endless number of cells.

Table 5: Values with respect to different mesh sizes

Mesh	Displacement	Cd
Fine	13.4	1.24
Medium	13.35	1.23
Coarse	10.22	1.20

The drag coefficient values for each of the three meshes are then compared to the Richardson extrapolated value, which is 1.245 and is displayed in Table 6, to determine the relative percentage inaccuracy. The medium mesh is selected as the optimal one by selecting the criteria to be 0.4 percent inaccuracy and computational time.

Table 6: Relative Error with respect to Richardson extrapolated value

Mesh	Cd	Relative Error(%)
Fine	1.24	0.4016
Medium	1.23	1.2048
Coarse	1.20	3.6145

3.2 Validation

3.2.1 Validation Against Schott et al. (2019) — Pulsating Flow Over a Bending Flexible Flap

To further validate the `solids4foam` implementation for more demanding FSI configurations, an additional benchmark case from Schott et al. [3] is reproduced. This case involves a highly flexible 3D flap subjected to pulsating inflow in a convection-dominated regime, representing a significantly more challenging test than the steady cross-flow case presented in Section 3.2.

3.2.1.1 Problem Description

The geometry comprises of a cuboid fluid domain $\Omega = [0, 1.8] \times [0, 0.6] \times [-0.6, 0.6]$ and a rubbery flexible flap with starting dimensions $\Omega^s = [0.5, 0.57] \times [0, 0.35] \times [-0.3, 0.3]$, clamped at the bottom wall at $x_2 = 0$. The flap material follows a neo-Hookean hyperelastic model with Young's modulus $E = 500$ Pa, Poisson's ratio $\nu^s = 0.4$, and density $\rho^s = 250$ kg/m³. The fluid properties are kinematic viscosity $\nu^f = 0.01$ m²/s and density $\rho^f = 1.0$ kg/m³, giving a Reynolds number ranging from 0 to 120 based on the maximum inflow velocity and flap width.

The inlet velocity follows a parabolic spatial profile modulated by a temporal factor:

$$u_1(\mathbf{x}, t) = g(t) \cdot u^{\max} \cdot \frac{2500}{81} x_2(x_2 - 0.6)(x_3 + 0.6)(x_3 - 0.6) \quad (6)$$

where $u^{\max} = 2.0$ m/s and the temporal modulation is defined as:

$$g(t) = \begin{cases} \frac{1}{2} (1 - \cos(\pi t)) & t \in [0, T_1 = 10.0] \\ 0 & t \in (T_1, T = 30.0] \end{cases} \quad (7)$$

This produces five inflow pulses that progressively excite the structure during $t \in [0, 10]$, followed by a free decay phase with no inlet flow. No-slip conditions are applied on all side walls, and a zero-traction Neumann condition is imposed at the outlet $x_1 = 1.8$.

3.2.1.2 Solver Configuration

The simulation is performed using `solids4foam` with a partitioned ALE approach, in contrast to the monolithic CutFEM formulation used by Schott et al. The fluid mesh is updated at each time step using the `velocityLaplacian` solver with quadratic inverse-distance diffusivity to preserve mesh quality during large structural deflections. A strongly-coupled implicit FSI loop with Aitken relaxation is employed, with a coupling tolerance of 10^{-6} and a maximum of 20 outer corrector iterations per time step. The temporal discretisation uses a backward Euler scheme with time step $\Delta t = 0.01$ s, and the convective term in the fluid momentum equation is discretised using a `linearUpwind` scheme to ensure stability at the higher Reynolds numbers encountered during peak inflow.

3.2.1.3 Monitoring Points

Following Schott et al. [3], the quantitative comparison is performed at the following monitoring locations:

- **Structural displacement:** point $\mathbf{X} = (0.5, 0.35, 0.0)$ (flap front top) and $\mathbf{X} = (0.57, 0.35, -0.3)$ (flap right top), both defined in the reference configuration, tracking the x_1 -component of displacement.
- **Fluid velocity magnitude and pressure:** point $\mathbf{x} = (0.6, 0.52, 0.0)$, located above the top surface of the deflecting flap.

3.2.1.4 Results and Comparison

Figure 7 shows the x_1 -displacement history at the flap front top point $\mathbf{X} = (0.5, 0.35, 0.0)$ and Figure 8 at the flap right top point $\mathbf{X} = (0.57, 0.35, -0.3)$ compared against the A2-mid discretisation of Schott et al. The present solids4foam result captures the qualitative response correctly: the structure bends progressively during the excitation phase ($t \in [0, 10]$), undergoes oscillatory motion driven by the pulsating inflow peaking near $t = 1, 3, 5, 7, 9$ s, and transitions to a free decay phase after $t = 10$ s when the inlet flow is removed.

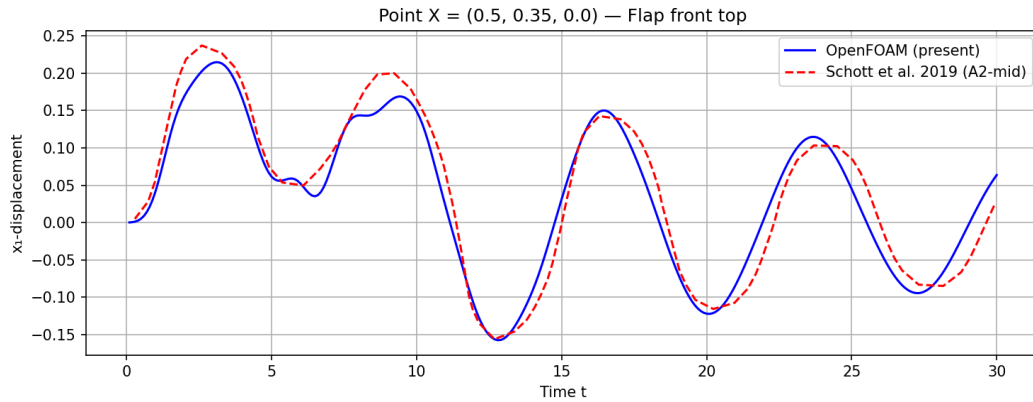


Figure 7: Comparison of x_1 -displacement at point $\mathbf{X} = (0.5, 0.35, 0.0)$: present solids4foam result versus Schott et al. [3] (A2-mid).

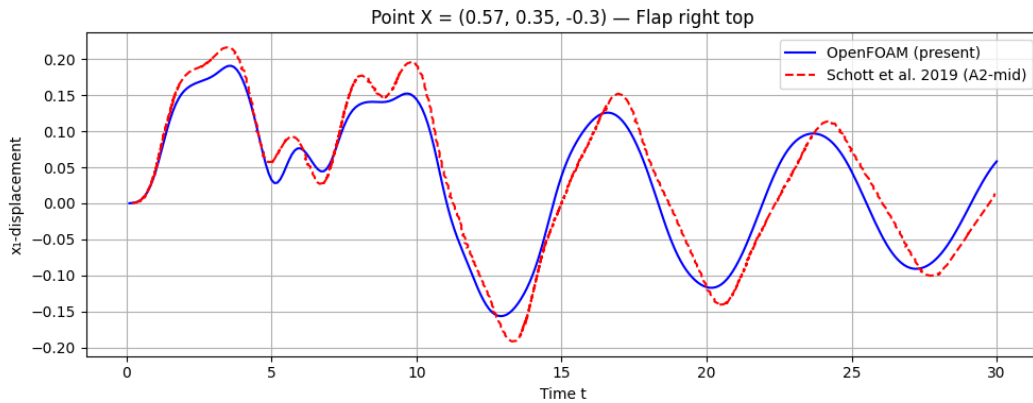


Figure 8: Comparison of x_1 -displacement at point $\mathbf{X} = (0.57, 0.35, -0.3)$: present solids4foam result versus Schott et al. [3] (A2-mid).

Figure 9 and Figure 10 show the fluid velocity magnitude and pressure histories respectively at the probe point $\mathbf{x} = (0.6, 0.52, 0.0)$. The reference solution exhibits sharp velocity peaks reaching approximately 1.8 m/s corresponding to each inflow pulse, with rapid decay after $t = 10$ s. The present results show good agreement in the oscillation frequency and the overall trend of the structural and fluid response.

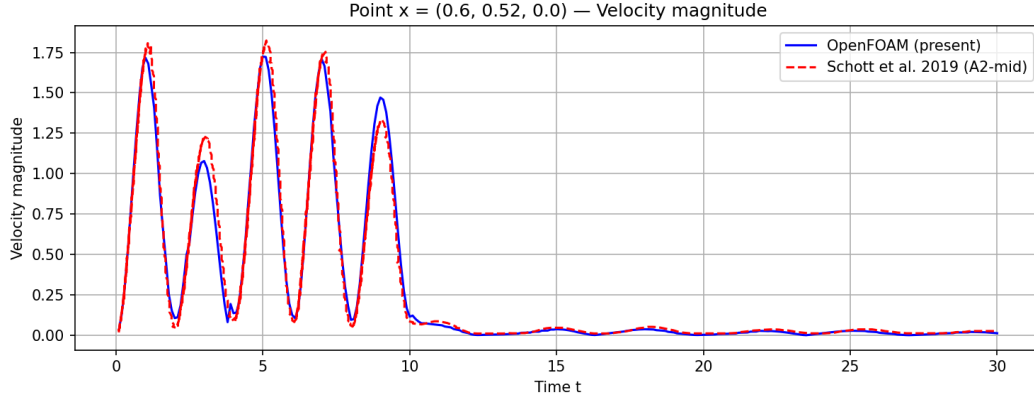


Figure 9: Comparison of fluid velocity magnitude at point $\mathbf{x} = (0.6, 0.52, 0.0)$: present solids4foam result versus Schott et al. [3] (A2-mid).

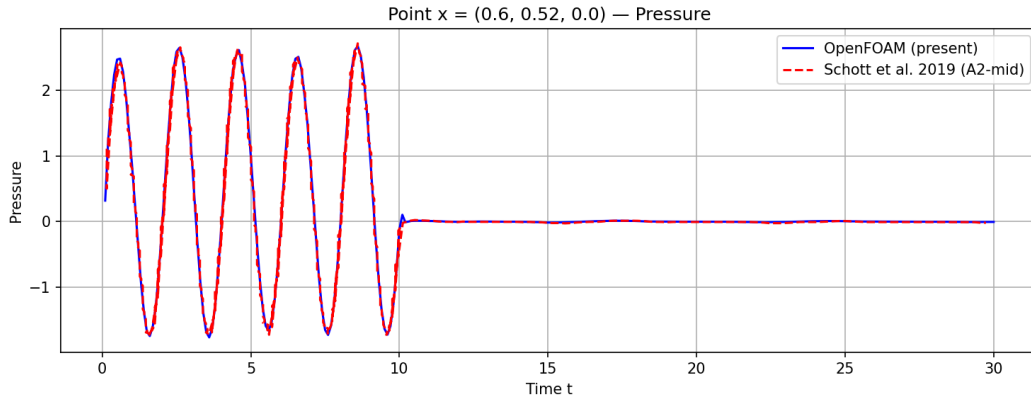


Figure 10: Comparison of fluid pressure at point $\mathbf{x} = (0.6, 0.52, 0.0)$: present solids4foam result versus Schott et al. [3] (A2-mid).

3.2.1.5 Summary

This benchmark demonstrates that solids4foam can reproduce the essential physics of pulsating flow-driven FSI with large structural deformations and convection-dominated flow at Reynolds numbers up to 120. The results provide additional confidence in the solver's applicability to transient, strongly-coupled FSI problems beyond the low-Reynolds-number steady-state regime.

3.3 Results

The flap's length scale is used to normalize the x direction displacement, and the mean inlet velocity and length scale are used to normalize the time. In our scenario, the length scale is 1 m and the average inlet velocity is 1 m/s. This makes it easier to compare data with flaps of various lengths. Figure 11 plots dimensionless displacement against dimensionless time and compares the findings with those from other solvers. In a similar manner, Figure 12 plots the drag coefficient versus normalized time and compares the results with those from other solvers. The flexible flap's displacement contours and the fluid domain's velocity contours are displayed concurrently in Figure 15. It displays the flap's position when the flow has fully developed and the flap achieves stable deflection. Similarly, Figure 13, Figure 14 and Figure 16 represents mesh morphing, velocity contour and streamline of the flow respectively.

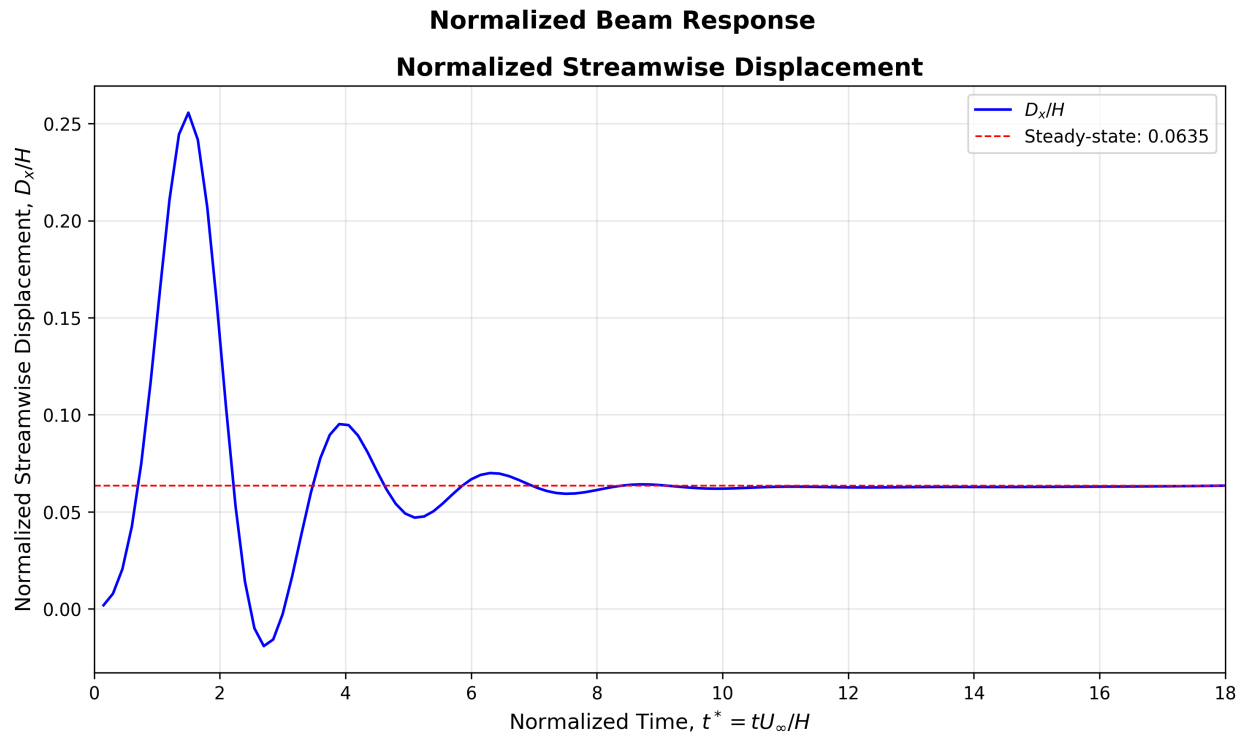


Figure 11: Normalised Displacement vs Normalised time

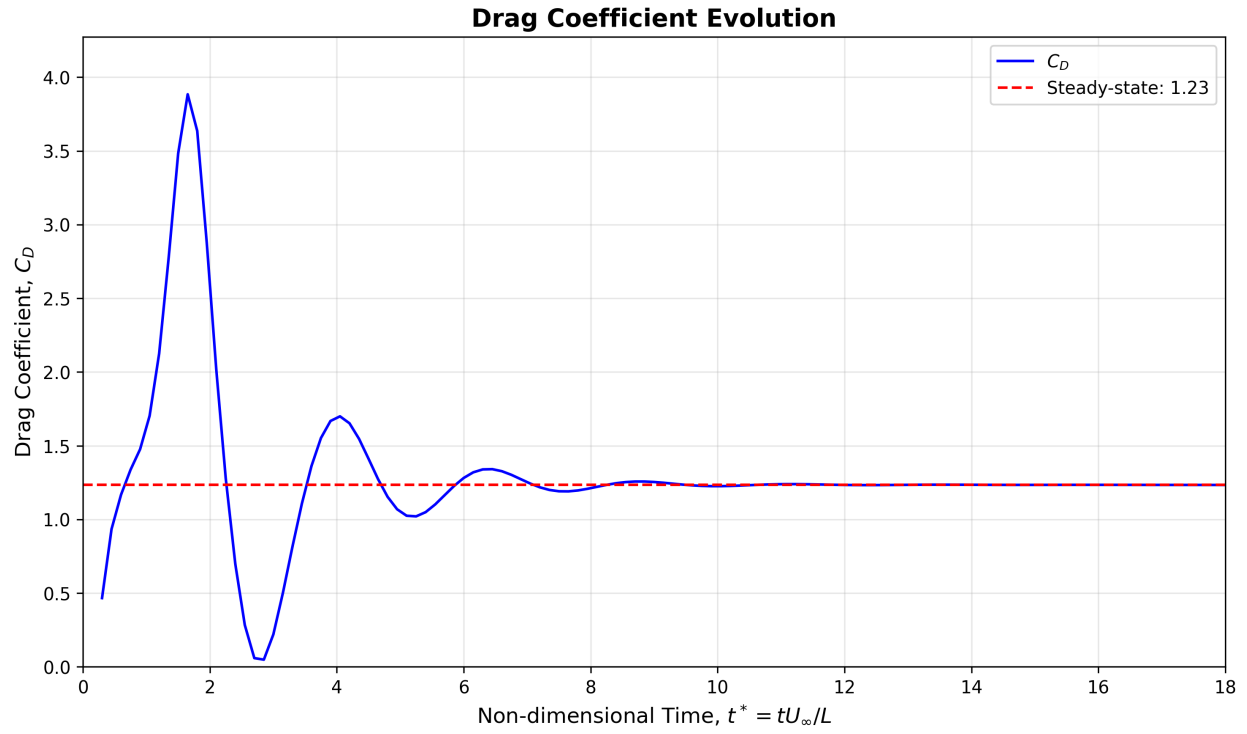


Figure 12: Coefficient of Drag(C_d) vs non-dimensionalised time

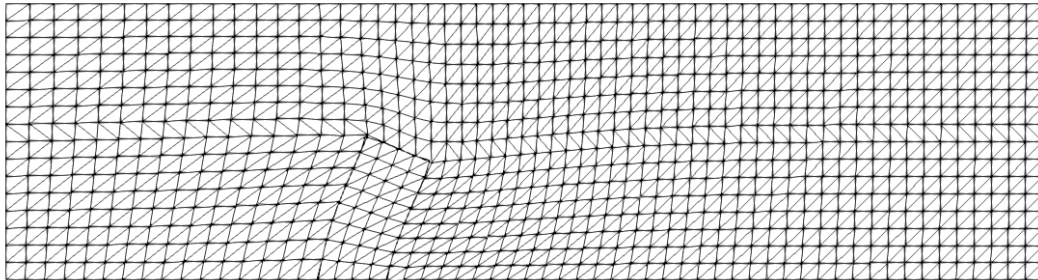


Figure 13: Mesh Morphing

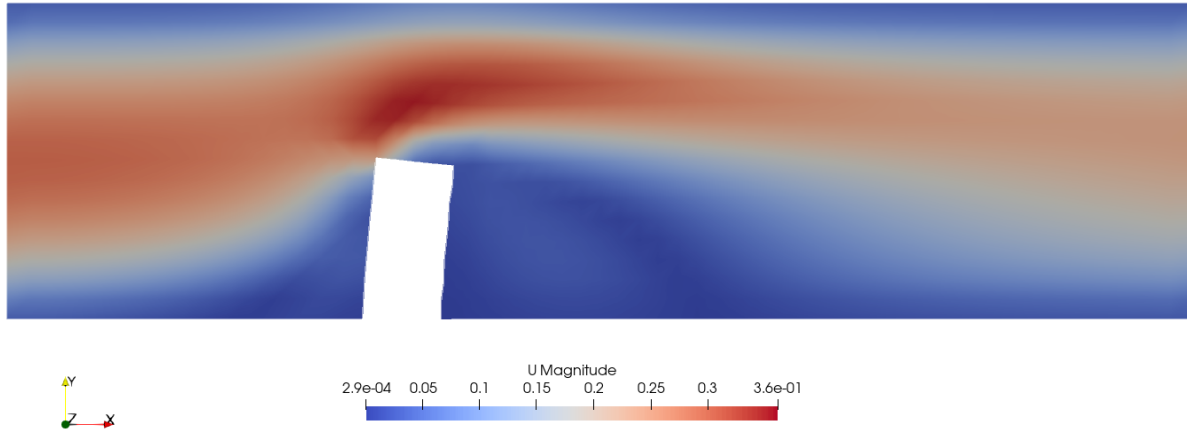


Figure 14: Velocity Contour

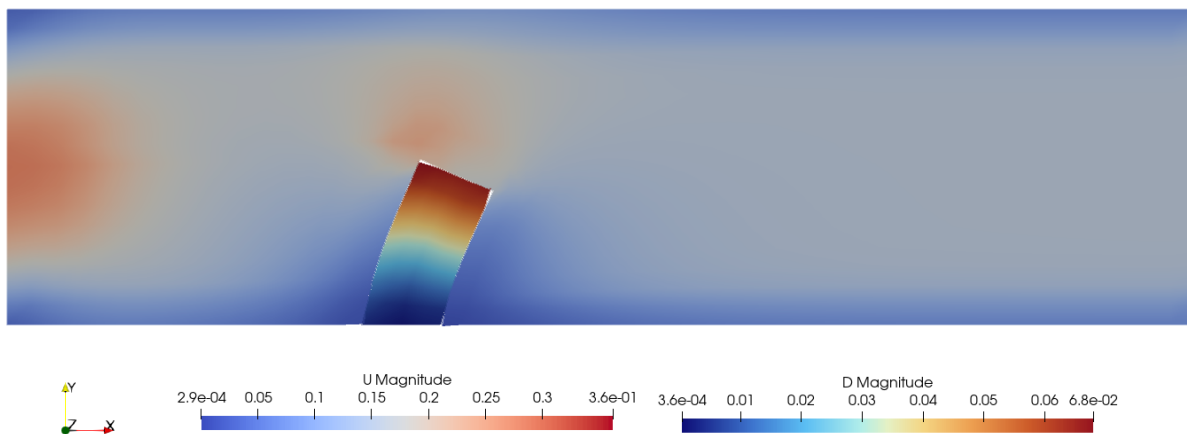


Figure 15: Displacement and Velocity Contour

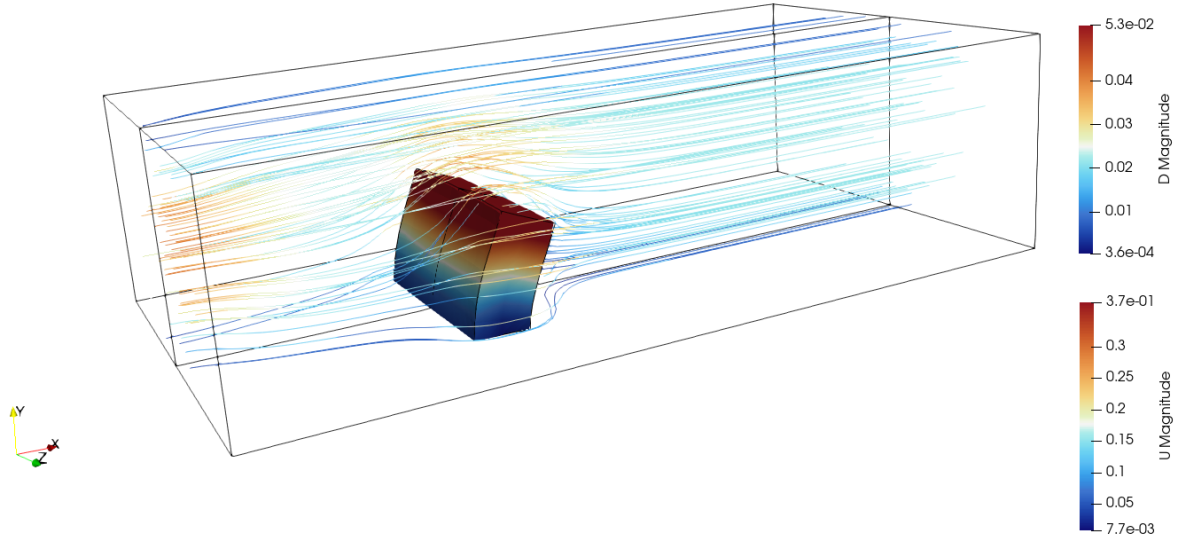


Figure 16: Streamline

3.3.1 Comparison with Original Case ($U = 0.2$ m/s, $E = 1.4$ MPa)

To validate the solids4foam implementation and understand the effect of flow velocity and material stiffness, a second simulation was conducted using the original case parameters as described in the tutorial [4]:

- Peak inlet velocity: $U_{max} = 0.2$ m/s
- Young's modulus: $E = 1.4$ MPa (shear modulus $\mu = 0.5$ MPa)
- Ramp-up time: $t_{ramp} = 4$ s

All other parameters remained identical to the modified case.

Figure 17 shows the drag coefficient evolution for both cases, while Figure 18 compares the normalized streamwise displacement.

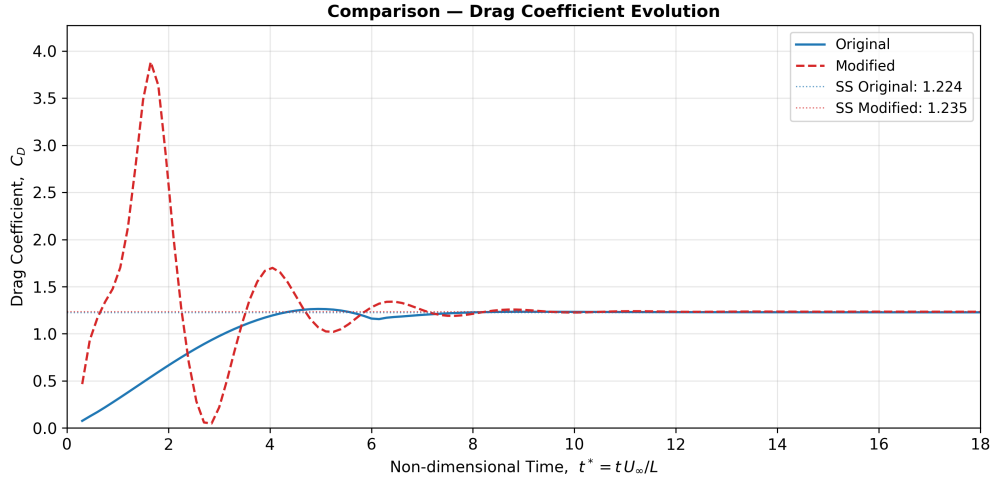


Figure 17: Comparison of Drag Coefficient: Modified Case ($U=0.3$ m/s, $E=10$ kPa) vs Original Case ($U=0.2$ m/s, $E=1.4$ MPa)

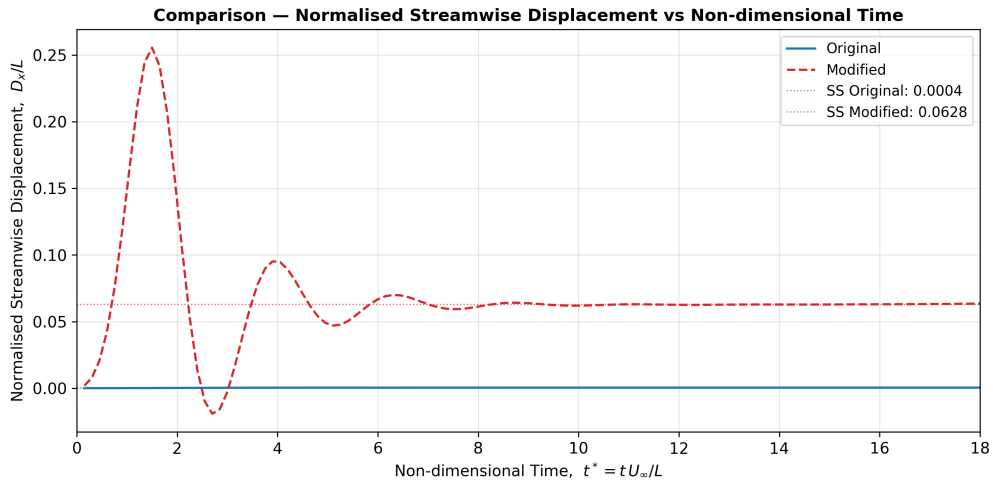


Figure 18: Comparison of Normalized Streamwise Displacement: Modified Case vs Original Case

3.3.1.1 Quantitative Comparison

Table 7 summarizes the steady-state values for both cases.

Table 7: Comparison of Steady-State Values

Parameter	Original Case	Modified Case	Ratio
Peak Inlet Velocity (m/s)	0.2	0.3	1.5
Young's Modulus (kPa)	1400	10	0.0071
Steady-state C_D	1.224	1.235	1.008
Steady-state D_x (mm)	0.1	13.35	133.5

3.4 Discussion

The modified case exhibits significantly larger deformation due to:

1. **Higher flow velocity:** 50% increase in inlet velocity results in approximately 4× higher dynamic pressure ($q = \frac{1}{2}\rho U^2$)
2. **Reduced stiffness:** Young’s modulus reduced by factor of 140, making the beam much more compliant

The combined effect leads to:

- Peak displacement larger in the modified case
- Longer settling time due to larger oscillations in the modified case

These results demonstrate the capability of solids4foam to handle a wide range of FSI problems, from small-deformation cases (original) to large-deformation, strongly-coupled scenarios (modified).

4 Conclusions

The solids4foam solver was used in this study to perform the FSI between the flexible perpendicular 3D flap and laminar incompressible flow. The flow Reynolds number is 40, and the density ratio of solid to fluid has been set at 1. The tolerance for the FSI loop inside each time-step has been maintained at 1e-6 in order to obtain the constant values of displacement and drag coefficient. The drag coefficient and displacement values oscillate when the tolerance values are greater than 1e-6.

5 Acknowledgement

First and foremost, I would like to sincerely thank my supervisor, Dr. Chandan Bose, whose outstanding guidance and insights during the project’s development were essential to its success and gave me a priceless learning opportunity. Without him, this project would not have been possible. Additionally, I would like to express my gratitude to Mrs. Payel Mukherjee, the FOSSEE team, and IIT Bombay for providing the chance, tools, and assistance required for the project’s success.

References

- [1] T. Richter, “A monolithic geometric multigrid solver for fluid-structure interactions in ale formulation,” *International journal for numerical methods in engineering*, vol. 104, no. 5, pp. 372–390, 2015.
- [2] Ž. Tuković, A. Karač, P. Cardiff, H. Jasak, and A. Ivanković, “Openfoam finite volume solver for fluid-solid interaction,” *Transactions of FAMENA*, vol. 42, no. 3, pp. 1–31, 2018.

- [3] B. Schott, C. Ager, and W. A. Wall, “Monolithic cut finite element–based approaches for fluid-structure interaction,” *International Journal for Numerical Methods in Engineering*, vol. 119, no. 8, pp. 757–796, 2019.
- [4] P. Cardiff, I. Batisti *et al.*, “solids4foam: A toolbox for performing solid mechanics and fluid-solid interaction simulations in openfoam,” *Journal of Open Source Software*, vol. 10, no. 108, p. 7407, 2025.
- [5] A. S. of Mechanical Engineers. Fluids Engineering Division, *Quantification of uncertainty in computational fluid dynamics*. American Society of Mechanical Engineers, 1993.